# DUAL-POLARIZED KU-BAND BACKSCATTER SIGNATURES OF HURRICANE OCEAN WINDS

Simon H. Yueh, Richard West, Fuk K. Li, Wu-Yang Tsai, and Rudy Lay

Jet Propulsion Laboratory
California Institute of Technology
4800 Oak Grove Drive
Pasadena, CA 91109
Tel: (818) 354-3012, Fax: (818) 393-3077

Submitted to IEEE Trans. Geosci. Remote Sensing in June 1998

**Abstract**

The Ku-band dual-polarized backscatter signatures of ocean surfaces are described in this article with the airborne scatterometer measurements collected in the Hurricane Ocean Wind Experiment in September 1997. The data collected from flights over Hurricane Erika provide a direct evidence that there are wind direction signals in the vertically and horizontally polarized Ku-band backscatter of ocean surfaces under the influence of hurricane force winds. At 46° incidence angle, the vertically polarized backscatter acquired at the upwind direction increases by about 1 dB as the wind speed increases from 22 $m \cdot s^{-1}$ to 35 $m \cdot s^{-1}$, while the horizontally polarized backscatter appears to be twice as sensitive with a change of about 2 dB. At 35 $m \cdot s^{-1}$ winds, the difference between upwind and crosswind observations of vertically polarized backscatter at 46° incidence angle is about 1.5 dB, smaller than the 2 dB difference for the horizontally polarized backscatter. This demonstrates that the horizontal polarization has a greater sensitivity to wind speed and direction than the vertical polarization in the high wind regime. The Ku-band airborne scatterometer data also suggest that the upwind and downwind asymmetry of Ku-band backscatter decreases with increasing wind speed and can fall below 0 dB at small incidence angles ($< 35°$) for the vertical polarization. A combined interaction of the geometric optics scattering and the short wave modulation by long ocean waves is proposed to interpret this phenomenon and appears to agree with the dependence of the signal on incidence angle, wind speed and polarization. The aircraft flight data support the feasibility of dual-polarized Ku-band radar for hurricane ocean wind measurements, although with a reduced wind speed and direction sensitivity in the high wind regime. Also the differing polarization backscatter signatures suggest the relative scattering contributions of long and short waves.

# 1 Introduction

The ocean surface wind measurements provided by the Special Sensor Microwave/Imager (SSM/I), Earth Remote Sensing Satellite (ERS) Advanced Microwave Instrument (AMI), and NASA Scatterometer (NSCAT) [1] data have shown a significant impact on the forecasting accuracy of numerical weather models. However, many studies have indicated that existing satellite microwave sensors systematically underestimate the ocean surface wind speed in the high wind regime [2, 3]. A significant speed bias in satellite surface wind measurements for high winds will undoubtedly affect their impact on the skill of storm forecasting models.

The accuracy of satellite wind velocities is determined by the accuracies of radar measurements and geophysical model functions. The radar measurement errors result from the uncertainties of instrument calibration, radar sensitivity, and propagation loss through the atmosphere. The errors caused by atmospheric losses can be significant at high winds typically associated with thick cloud cover and rain. Besides the radar measurement errors, the other major error source for wind retrieval at high winds is the uncertainty of the geophysical model functions (GMF).

The GMF for satellite wind scatterometers relates the radar backscatter to the surface wind velocities [4, 5]. Lately, a technique that has been widely used for the derivation of the GMF for spaceborne radars utilizes the numerical weather model winds as input fields. For example, the C-band GMF (CMOD4) developed for the European Space Agency (ESA) is based on the colocated European Centre for Medium-Range Weather Forecasts (ECMWF) analysis field and ERS-AMI measurements [13]. CMOD-IFR2, the GMF used for the off-line wind scatterometer processing by the French Processing and Archiving Facility, also results from a similar analysis of ECMWF fields together with a selected set of buoy data [2]. The same technique has also been employed by the NSCAT science team to obtain the first operational GMF for NSCAT, hereafter referred to as the NSCAT-1 GMF. There is a reasonable agreement at low and moderate wind speeds ($<20$ m$\cdot$s$^{-1}$) between CMOD4 and

CMOD-IFR2, but the difference is significant at higher wind speeds. This suggests that there is a lack of reliable high wind ECMWF analysis and buoy dataset at above 20 $m \cdot s^{-1}$. Additionally, many studies have shown that the ERS-1 scatterometer products derived from CMOD4 significantly underestimate the wind speed of tropical storms. For instance, Rao et al. [3] analyzed the ERS-1 observations over a cyclone system in the Bay of Bengal and found that the maximum scatterometer wind speed is 25 $m \cdot s^{-1}$, significantly less than the maximum sustained wind speed of around 50 $m \cdot s^{-1}$ estimated from the geostationary satellite imagery. Similar conclusions were reached by [2] with the analysis of ERS-1 passes over Typhoon Elsie (November 1992). Their findings are consistent with the airborne scatterometer measurements of hurricane winds [20], which indicated that CMOD4 significantly overestimates ocean backscatter at high winds (20 to 30 $m \cdot s^{-1}$). It was hypothesized that the biases in CMOD4 and CMOD-IFR2 for high winds are related to an improper extrapolation by both models with the model coefficients apparently invalid at high wind speed (above 15 $m \cdot s^{-1}$) [2]. As to be shown in this article, the weakness of numerical model winds for the development of satellite scatterometer GMF in the high wind regime is also reflected in the NSCAT-1 GMF.

The aircraft flights conducted by the University of Massachusetts (UMASS) through Hurricane Tina in September 1992 [20], probably the first successful airborne scatterometer hurricane campaign, operated C-band vertically polarized scatterometers with the surface wind speed indirectly inferred from another microwave sensor, the Stepped Frequency Microwave Radiometer (SFMR), which has no wind direction measurement capability. To explore the polarization signatures of Ku-band ocean backscatter and polarimetric microwave radiometer signals at high winds with direct in situ measurements, the Hurricane Ocean Wind Experiment (HOWE) was organized by the Jet Propulsion Laboratory (JPL) in conjunction with the Naval Research Laboratory (NRL) with a set of aircraft flights over Hurricane Erika in September 1997. The HOWE sensor suite includes the JPL Ku-band dual-polarized scatterometer (NUSCAT), JPL polarimetric wind radiometers (17, 19, and 37 GHz), NRL

X-band polarimetric radiometer, UMASS C- and Ku-band scatterometers, and the contributions from several other institutions. The surface truth was obtained by a direct measurement of wind velocity (speed and direction) along with several meteorological parameters with the GPS dropsondes, representing an improvement over the earlier aircraft scatterometer campaign for hurricane wind studies [20]. As to be shown later, the vertical and horizontal polarizations of ocean backscatter at hurricane force winds (>32 $m \cdot s^{-1}$) have distinct upwind and downwind asymmetries. A direct wind direction measurement acquired by the GPS dropsondes helps strengthen the validity of our observations.

This article will describe the characteristics of Ku-band ocean backscatter acquired by the JPL NUSCAT from the HOWE deployment under high wind conditions. Section 2 describes the characteristics of NUSCAT. The field experiments conducted over a period of two years were described in Section 3. The behaviors of the Ku-band ocean backscatter from the field experiments are presented in Section 4. Summary is given in Section 5.

# 2 NUSCAT

To study the ocean radar backscatter over a range of environmental conditions, an airborne Ku-band (13.95 GHz) scatterometer (NUSCAT) was developed at the Jet Propulsion Laboratory. The key parameters of NUSCAT for the HOWE deployment are described in Table 1. NUSCAT employs a two-axis gimbal to point the parabolic reflector antenna at any incidence (0° to 65°) and azimuth angles. During aircraft level flights, the antenna is scanned in azimuth with a typical step size of 10° at a selected incidence angle. The gimbal control also allows the operation of NUSCAT for circle flights with the antenna pointing to a fixed direction (the starboard of the aircraft for right hand banks). To improve the signal detection sensitivity ($K_p$) [14], the transmit frequency of NUSCAT can be hopped within +/- 50 MHz bandwidth centered at 13.95 GHz from pulse to pulse so that the radar echos from several consecutive transmit pulses are uncorrelated: The resulting $K_p$ is about 0.2 dB for an integration time of 0.5 seconds with a pulse repetition frequency of 1500 Hz. NUSCAT can

transmit horizontal or vertical polarizations and receive both polarizations simultaneously, and hence can acquire dual-polarized radar backscatter to support the development of a dual-polarized GMF for NASA Scatterometers (NSCAT and SeaWinds). Prior to 1997, NUSCAT could only operate one transmit polarization for each flight line and required two passes over the same area to acquire VV and HH backscatter data [19]. For the HOWE deployment in September 1997, the NUSCAT command and data system was modified to alternate vertical and horizontal transmit polarizations for every 5 seconds so that $\sigma_{vv}$ and $\sigma_{hh}$ can be acquired over nearly the same areas to enable a better comparison of dual-polarized ocean backscatter signatures.

The calibration of NUSCAT transmit power and receiver gain was performed using a loop-back technique with a small percentage of transmit power leaked into the receiver once per every 10 minutes to remove the drift of transmit power and receiver gain during flight operations. This technique has been used in the NASA SeaWinds scatterometer and many other airborne and spaceborne radar systems. Laboratory tests suggest that the calibration stability of this technique for NUSCAT is better than 0.2 dB.

The absolute calibration of NUSCAT was achieved by adjusting the system calibration factor to make the normalized radar cross sections ($\sigma_0$) acquired at 10° incidence angle equal 6.3 dB, which is interpolated from the Seasat scatterometer geophysical model function [5]. This adjustment appears to provide a good agreement between the NUSCAT flight data and the NSCAT-1 GMF at low and moderate wind speeds (Figs. 2 and 6). Because NUSCAT uses independent waveguides for the vertical and horizontal polarization channels from the radio frequency electronics to the antenna, laboratory measurement errors of the waveguide loss, rotary joint loss, and antenna gain contribute to errors in the relative gain of these two polarization channels. The balance of vertical and horizontal polarization channels was achieved by performing data acquisition at 0 degree incidence angle over ocean surfaces with the transmit polarization alternating between vertical and horizontal polarizations. Because the ocean backscatter is expected to be the same at normal incidence angle for

both polarizations, the difference between VV and HH backscatter indicates the imbalance between vertical and horizontal polarization channels and is used to adjust the gain of the NUSCAT horizontal polarization channel.

# 3 Field Experiments

In November 1996, NUSCAT was deployed on the NASA P-3 with four flights over the National Oceanic and Atmospheric Administration (NOAA) National Data Buoy Center (NDBC) buoys in the Atlantic. The flight pattern over each selected buoy consisted of one level flight and three sets of circle flights with a constant bank angle of 10°, or 20°, or 30°, leading to 50°, 40°, and 30° incidence angles. Because the ferrite switch for transmitting horizontal polarization failed during the flights, the data acquisition was limited to vertical polarization measurements. For this deployment, the traveling wave tube amplifier (TWTA) was used for transmit with a peak power of about 100 watts, which produces a signal to noise ratio (SNR) of about 10 dB for 3 $m \cdot s^{-1}$ winds at 50° incidence angle and 26,000 ft altitude. The buoy wind speeds for these four flights were in the range of 3 to 15 $m \cdot s^{-1}$ with cloud overcast for all cases. There was a two-frequency (19 and 37 GHz) polarimetric radiometer flown together with NUSCAT and the radiometer data were used to estimate the loss of atmosphere at Ku-band. The estimated atmospheric losses (one way) at 55° incidence angle at NUSCAT frequencies were less than three tenths of a dB for most cases. The only exception is the last data flight over NDBC buoy 41001, where there were thick stratus clouds with the loss reaching about 0.5 dB one way.

During the HOWE in September 1997, NUSCAT was flown together with many other passive microwave radiometers on the NASA P-3 research aircraft. Two flights over Hurricane Erika were performed on September 10 and 11, 1997. Additional data were acquired over the NDBC buoy 44004 during the transit flight from Bermuda to the Wallops Island on September 12, 1997. Hurricane Erika reached its peak intensity of 110 knots on the 8th of September and retained this wind speed for a period of 24 hours, while it was located

300 nautical miles north of the Caribbean islands. It was a category three hurricane on the Saffir/Simpson Hurricane scale. The hurricane passed about 300 nautical miles east of Bermuda on the 10th and turned toward the east-northeast on the 11th and 12th. The maximum wind speed estimated from the geostationary satellite imagery during the time of the aircraft flights was about 80-90 knots (40-45 $m \cdot s^{-1}$) on the 10th and 65-70 knots (32-35 $m \cdot s^{-1}$) on the 11th [6]. This flight campaign was specifically designed for on-board passive microwave radiometers which require circle flights. Most of the NUSCAT data were acquired with the antenna boresight pointing to the starboard of P-3 for data collection at 35, 46, and 54 degree incidence angles. However, two straight level flight legs with a bow-tie flight pattern were also performed for each target site for other microwave instruments. The NUSCAT data from level flights agreed very well with those from circle flight operations. Given the nominal flight altitude of 21,000 ft, the agreement between level and circle flight data suggest that the surfaces were quite uniform within a range of 5-10 km.

During the Erika flights, the GPS dropsondes were launched from P-3 to acquire the surface truth. GPS dropsondes provide the measurements of the wind speed and direction (horizontal components), pressure, temperature, and humidity for every 0.5 seconds, while descending through the atmosphere. For the meteorological data, including pressure, temperature, and humidity, the sonde first samples the sensors during a half second interval and transfer the raw data counts to a memory buffer for transmission in the next half second interval. Because of the buffering, the last sampled point is never transmitted out after splash so that the last measured data point received by the aircraft data system is the second to last point sampled, which is at a minimum, 0.5 seconds or 6 m above the water. It is simpler for the wind data: The wind measurement is a 'flash' measurement of the GPS Doppler registers in the sonde but there is a mean delay of 0.26 seconds.

Fig. 1 illustrates the dropsonde data acquired from the NASA P-3 hurricane flights at two locations (A and B). The upper right panel plots the vertical velocity of the dropsonde versus altitude, indicating that the vertical velocity of the dropsonde was about 12 $m \cdot s^{-1}$

near the surface. This suggests that the last dropsonde measurement, transmitted to the aircraft dropsonde control rack before the dropsonde plunged into the water, was acquired at a few meters above the surface. Location A had a strong surface wind speed (about 35 $m \cdot s^{-1}$) and there apparently was a strong convection resulting in a well-mixed layer indicated by a fairly uniform wind speed within a few hundred meters above the surface. Therefore it is unnecessary to apply the boundary layer conversion of the near surface wind speeds between different elevations [15]. A high surface wind speed suggests that location A was quite close to the eye of hurricane with a high near surface humidity and a low surface pressure (about 970 mb). Location B was further away from the eye with a higher surface pressure ($\sim$ 1000 mb) and lower surface wind speed (about 22 $m \cdot s^{-1}$). These two locations were intentionally selected to be off rain bands by the aircraft pilots during flights, and hence heavy rains were not expected in both regions: The two-way atmospheric attenuation at 45° incidence angle estimated from coincidental radiometer data are about 0.8 and 0.6 dB, respectively, for these two locations.

Regarding the accuracy of dropsonde winds, a GPS dropsonde was launched during the transit flight over the NOAA buoy 44004 on September 12, 1997. The buoy wind speed was 9.4 $m \cdot s^{-1}$ at 211° from the north at 5 m elevation, while the dropsonde wind speed was 11.5 $m \cdot s^{-1}$ at 216.84°. The agreement in wind direction is remarkable, but there is a wind speed difference of about 2 $m \cdot s^{-1}$. Part of the difference could be due to the difference between their measurement techniques. This flight test suggests an accuracy about $\pm 2$ $m \cdot s^{-1}$ for dropsonde winds.

Aircraft navigation data for both sets of flights indicated that the aircraft bank angles were always maintained to within $\pm 1°$. Based on the aircraft attitude data, the actual incidence angle of each backscatter sample was calculated and used to correct the variations of incidence angles: First, the difference of the actual and desired incidence angles was used to estimate the difference of backscattering coefficients at these two incidence angles based on the data acquired at three incidence angles over the same locations. The resulting estimates

of backscatter corrections are smaller at higher incidence angles, ranging from about 1 dB at low winds to about 0.1 to 0.2 dB at 35 $m \cdot s^{-1}$ winds. Since the accuracy of aircraft attitude data is about 0.1° (10 percent of the control accuracy of 1°), the residual calibration errors are expected to be less than 10 percent of the estimated corrections, i.e., about 0.02 dB at 35 $m \cdot s^{-1}$ winds.

# 4 Data and Discussions

As an evaluation of the relative calibration accuracy of NUSCAT and NSCAT backscatter measurements, Fig. 2 compares NUSCAT $\sigma_{vv}$ measurements from November 1996 flights with the NSCAT-1 GMF at low and moderate winds. The agreement is reasonable for most data points. In the wind speed range of 13 to 16 $m \cdot s^{-1}$, the comparison indicates that the NSCAT-1 GMF provides a slightly higher backscatter than the NUSCAT data at all incidence angles. As to be shown later, this trend appears to extend into higher wind speeds (Fig. 6). It appears that the NUSCAT backscatter is noisy at low winds, probably due to the influence of other surface parameters, such as swell and surface temperatures [19], which affect the generation of short-gravity and capillary waves and consequently the radar cross sections. The analysis of NSCAT backscatter by the NSCAT science team also indicates a larger scatter at lower winds, consistent with the NUSCAT observations. In any case, a reasonable agreement suggests that the relative calibration between NUSCAT and NSCAT is within 1 dB.

The wind speeds reported by the GPS dropsondes for two Hurricane Erika flights were in the range of 20 to 35 $m \cdot s^{-1}$. Figs. 3 and 4 illustrate the NUSCAT $\sigma_{vv}$ and $\sigma_{hh}$ data as a function of azimuth angle at 35° and 46° incidence angles. The backscatter data were acquired at 22 and 35 $m \cdot s^{-1}$ winds at locations A and B with the GPS dropsonde measurements plotted in Fig. 1. There were clear wind direction signals with the azimuth angles of backscatter peaks in excellent agreement with the GPS dropsonde wind directions. Comparing the measurements at these two wind speeds suggests that the azimuthal modulations

of $\sigma_{vv}$ and $\sigma_{hh}$ decrease with increasing wind speed. This is possibly due to a more isotropic directional spreading of short gravity and capillary waves at higher wind speeds [11].

Although the surfaces were expected to be highly perturbed under the influence of storm and hurricane force winds, there are distinct polarization behaviors: The horizontal polarization is more sensitive to the wind speed and direction than the vertical polarization. It is shown in Fig. 3 that $\sigma_{hh}$ has a stronger azimuthal modulation than $\sigma_{vv}$ by about 25 percent with an upwind and crosswind asymmetry of about 4 dB for $\sigma_{hh}$ and about 3 dB for $\sigma_{vv}$ for 22.2 m·s$^{-1}$ wind at 46° incidence. The difference is smaller at 35° incidence angle (Fig. 4) with more similar directional modulations in both polarizations. The horizontal polarization also has a stronger wind speed sensitivity than the vertical polarization at 46° incidence angle: Comparing the upwind backscatter acquired at 22 and 35 m·s$^{-1}$ wind speeds suggests that $\sigma_{hh}$ at upwind directions changes by about 2 dB versus the 1 dB change for $\sigma_{vv}$ between these two wind speeds. A stronger wind velocity sensitivity at high winds for the horizontal polarization could be the results of scattering from breaking waves: As suggested by the ground-based radar measurements [16], the backscatter from breaking waves is polarization insensitive and is roughly proportional to the cubic power of friction velocity ($u*$) for wind speeds up to at least about 15 m·s$^{-1}$. By comparison, the NSCAT-1 GMF suggests that $\sigma_{vv}$ and $\sigma_{hh}$ at low and moderate winds (3 to 10 m·s$^{-1}$) presumably dominated by the Bragg scattering are roughly proportional to the square of wind speed (Fig. 6), rising less rapidly than the contribution by breaking waves. Because of a weaker Bragg scattering for the horizontal polarization, the percentage contribution of breaking waves is about 15 percent for $\sigma_{hh}$ and about 8 percent for $\sigma_{vv}$ at about 15 m·s$^{-1}$ [16]. If the percentage contribution of breaking waves continue to increase at higher wind speeds, it is conceivable that $\sigma_{hh}$ would have a stronger wind speed sensitivity than $\sigma_{vv}$ in the high wind regime. However, it appears that the Bragg scattering remains to be the dominant scattering mechanism at moderate and high incidence angles. Otherwise, $\sigma_{hh}$ and $\sigma_{vv}$ should have a similar wind speed sensitivity if the breaking waves become dominant.

An interesting signature indicated in Fig. 4 is the upwind and downwind asymmetry of $\sigma_{vv}$ and $\sigma_{hh}$ at 35 m·s$^{-1}$ wind speed: The upwind measurements of $\sigma_{vv}$ is smaller than the downwind observations, while there is no apparent asymmetry in the $\sigma_{hh}$ data. This behaviour in $\sigma_{vv}$ is markedly different from that shows at low to moderate wind speeds in the NSCAT-1 GMF, in which the upwind $\sigma_{vv}$ is higher than the downwind $\sigma_{vv}$. The rationale for a negative upwind and downwind $\sigma_{vv}$ asymmetry for high winds will be further explored during the discussion of the data presented in Fig. 7.

Another useful parameter indicating the relative significance of surface scattering mechanisms is the polarization ratio ($\sigma_{vv}/\sigma_{hh}$). Fig. 5 illustrates the polarization ratio versus wind speed for NUSCAT data and the NSCAT-1 GMF. The polarization ratio in dB is positive and has a decreasing trend with increasing wind speed for all incidence angles. It is apparent that there is a larger polarization ratio at higher incidence angles. The polarization ratio at 35° incidence is quite significant at about 10 m·s$^{-1}$ winds, but becomes closer to unity at higher winds. In contrast, the polarization ratio at 54° incidence remains quite significant (about 1.5 dB) at high winds. It is known that the polarization ratio of the geometric optics backscattering from long ocean waves and the diffused backscattering from breaking waves is close to unity (or 0 dB) [16], while the Bragg scattering can produce a few dB polarization ratio at high incidence angles. The magnitude of polarization ratio depicted in Fig. 5 suggests that the Bragg scattering by small scale waves remains dominant at incidence angles $> 40°$ in the high wind regime, but the geometric optics scattering and breaking waves are more significant at 35° incidence.

Fig. 6 illustrates the upwind and crosswind dual-polarized backscatter from NUSCAT and the NSCAT-1 GMF at 35°, 46°, and 54° incidence angles. The radio propagation loss through the atmosphere estimated from the passive microwave radiometer measurements collected at the same time is typically less than 1 dB and has been used to correct the NUSCAT data. It is apparent that there is a significant discrepancy between the NSCAT-1 GMF and the NUSCAT data at above 20 m·s$^{-1}$ winds. If the NSCAT-1 GMF is used to

estimate the wind speed from NUSCAT data, the hurricane force winds ($> 32$ m·s$^{-1}$) could be underestimated by more than 10 m·s$^{-1}$, which is far beyond the expected accuracy of GPS dropsonde winds. The NUSCAT data show that the NSCAT-1 GMF requires a substantial correction for hurricane winds.

In general, the NUSCAT backscatter rises less rapidly with wind speed at high winds than at low and moderate winds. This characteristic is consistent with the C-band radar observations of hurricane ocean winds [20]. If we assume a power law model of the form $\alpha U_{10}^{\gamma}$ to fit the upwind radar backscatter, it is straightforward to show that $\gamma$ for the NSCAT-1 GMF is about 2.1 in the range of wind speed from 3 to 12 m·s$^{-1}$ at above 40° incidence angles, the regime where the Bragg scattering by small scale roughness is expected to be dominant. ($U_{10}$ is the wind speed at 10 meter height.) However, the NUSCAT data suggest that $\gamma$ is closer to unity at 46° incidence at above 20 m·s$^{-1}$. A decreased wind speed sensitivity of the radar backscatter with wind speed in the high wind regime could be due to a gradual saturation of surface roughness resulting from the breaking of short gravity and capillary waves [17, 18].

Fig. 7 illustrates the upwind/crosswind and upwind/downwind asymmetries of $\sigma_{vv}$ and $\sigma_{hh}$. The hurricane flight data are indicated by open circles and crosses. The data indicated by the filled black circle and plus are interpolated from the NUSCAT flight data collected in 1996. Because the flights in November 1996 were conducted at 30°, 40°, and 50° incidence angles, the upwind/crosswind and upwind/downwind asymmetries were derived at those angles and interpolated to 35° and 46°. There is a reasonable agreement between the NSCAT-1 GMF and NUSCAT data. (A noisy NSCAT-1 GMF for the HH backscatter suggests that three months of colocated NSCAT horizontally polarized backscatter data and numerical model winds are insufficient to reduce the statistical uncertainty.) The upwind/crosswind asymmetry decreases with increasing wind speed at above 7 m·s$^{-1}$. The NUSCAT data are quite noisy at low winds, likely due to a more random fluctuation of winds and a stronger impact of other oceanic parameters at lower wind speeds [19]. As discussed earlier, this

characteristic is consistent with what has been noted in the NSCAT data by the NSCAT Calibration and Validation Team: It was found that NSCAT backscatter data grouped into 50 km resolution bins have larger deviations from the NSCAT-1 GMF at lower wind speeds.

It is noted in Fig. 7 that there are two outliers in the plot of $\sigma_{hh}$ data at 54° incidence with an upwind/crosswind asymmetry of about 6 dB, while the coincidental $\sigma_{vv}$ data do not show such a strong signal. This indicates that $\sigma_{hh}$ is influenced by other surface phenomena, which do not have as strong an impact on $\sigma_{vv}$ at a high incidence angle ($> 50°$). It is speculated that this stronger-than-expected directional signal in $\sigma_{hh}$ is caused by the breaking waves, which have a relatively stronger influence on the horizontal polarization than the vertical polarization [21].

There is a very intriguing phenomenon regarding the wind speed, polarization, and incidence angle dependence of the upwind and downwind asymmetry. It has been suggested by many studies that the upwind and downwind asymmetry of ocean radar backscatter is caused by the asymmetric distribution of short gravity and parasitic capillary waves (small scale waves) on the windward and leeward faces of long waves [11, 12]. Both NSCAT and NUSCAT data suggest that the upwind and downwind asymmetry reduces with increasing wind speed at low and moderate winds. This is likely due to a more symmetric distribution of parasitic capillary waves and/or the more likely breaking of small scale waves at higher wind speeds. What is unexpected is that as the wind speed exceeds 20 $\mathrm{m{\cdot}s^{-1}}$, the NUSCAT data suggest a negative upwind and downwind asymmetry for $\sigma_{vv}$ at 35° incidence angle. (An artificial threshold has apparently been applied in the NSCAT-1 GMF to limit the asymmetry of $\sigma_{vv}$ to 0 dB at above 15 $\mathrm{m{\cdot}s^{-1}}$ wind speed. It appears that a straight extrapolation of the NSCAT-1 GMF predictions from less than 15 $\mathrm{m{\cdot}s^{-1}}$ will fall through the NUSCAT high wind data.)

It is quite well-accepted that the upwind and downwind asymmetry of ocean backscatter is due to an asymmetric distribution of small scale ocean waves on the faces of long waves. It has been observed that the small scale ocean waves are more concentrated on the leeward

faces of long waves than the windward faces [11, 12], at least for low and moderate winds: This will result in a stronger Bragg scattering at the upwind observation directions than the downwind directions [9, 10]. Therefore, in view of the NSCAT-1 GMF and NUSCAT data it seems obvious to assume that there are more small scale ocean waves on the leeward faces of long waves than the windward faces for low and moderate winds, and the sign change in the upwind and downwind asymmetry would suggest that the small scale waves become more concentrated on the windward faces of long waves as the wind speed becomes very high. There are, however, problems with this assumption. It is known that the horizontal polarization is more sensitive to the spatial distribution of small scale waves than the vertical polarization, and consequently $\sigma_{hh}$ has a bigger upwind and downwind asymmetry than $\sigma_{vv}$ for low and moderate winds. If there are more small scale waves on the windward faces, the Bragg scattering should result in a more negative upwind and downwind asymmetry for $\sigma_{hh}$ than for $\sigma_{vv}$. However, this is opposite to what is observed in the NUSCAT dual-polarized backscatter data for high winds. The other problem is that the incidence angle dependence of the upwind and downwind asymmetry resulting from the redistribtuion of the small scale waves is not supported by the NUSCAT data. At low and moderate wind speeds, the Bragg scattering from small scale waves produces an increasing upwind and downwind backscatter asymmetry with incidence angle. Should there be more small scale waves on the windward faces, the Bragg scattering should produce a more negative backscatter asymmetry at higher incidence angles. However, the NUSCAT data suggest that the upwind and downwind asymmetry of $\sigma_{vv}$ and $\sigma_{hh}$, remains positive and increase with incidence anlges. Therefore, the assumption that the small scale waves are more concentrated on the windward faces at high winds does not seem to offer radar signatures consistent with the experimental observations.

Another possible interpretation involves the relative contribution of geometric optics (GO) scattering from long waves and the Bragg scattering from small scale waves [9]. The GO scattering is due to the long waves with their surfaces normal to the radar look direction,

and its contribution is proportional to the probability of surface slopes and the reflectivity of the long waves. For off-nadir GO backscatter, the leeward (windward) faces of long waves contribute to the upwind (downwind) radar observations. Because of the presence of small scale waves, the surface reflectivity of long waves decrease with increasing wind speed. (This is evident in the spaceborne altimeter measurements of ocean radar cross sections.) If there are more small scale waves on the leeward faces of long waves than the windward faces, the upwind GO backscatter will be smaller than the downwind GO backscatter, and consequently the GO scattering from long waves will result in a negative contribution to the upwind/downwind asymmetry. In contrast, the upwind/downwind asymmetry resulting from the Bragg scattering is positive, increases with increasing incidence angles and is larger for horizontal polarization than vertical polarization, if there are more small scale waves on the leeward faces. Under low and moderate wind conditions, the Bragg scattering, apparently dominating the ocean backscatter at moderate and high incidence angles, would lead to a positive upwind and downwind asymmetry. When the wind speed increases, resulting in an increase of long wave slopes, the GO scattering becomes more significant and could become comparable to the Bragg scattering. Because the GO scattering has a stronger impact at a lower incidence angle, this interpretation will explain why the upwind and downwind asymmetry is more likely to be negative at 35° incidence angle than higher incidence angles. Additionally, because $\sigma_{hh}$ has a larger upwind/downwind asymmetry than $\sigma_{vv}$ due to the Bragg scattering, the GO scattering, which is polarization insensitive, can reduce the upwind/downwind asymmetry of $\sigma_{hh}$, but is insufficient to overturn the contribution of Bragg scattering at above about 40° incidence.

In the following, we attempt to examine the contribution of the GO scattering in a more quantitative way with some assumptions about the roughness of ocean surfaces. It should be aware that our present knowledge of the wind wave spectrum is very limited in the high wind regime. Therefore, the following analysis should only be considered as a numerical demonstration of the effects of the GO scattering described above. Accurate measurements

of the ocean surface spectrum and the modulation of small scale waves by long waves at high winds are needed to validate the results from the analysis.

To proceed, we will assume a Gaussian distribution for the slopes of long waves. Under this assumption, the contribution of GO scattering [9] to the backscattering coefficients at an incidence angle $\theta$ can be written as

$$\sigma_{GO} = \frac{|R_0|^2}{2S_u S_c} \sec^4\theta \exp(-\frac{\tan^2\theta}{2S_u^2}) \exp(-4k_0^2h^2) \tag{1}$$

where $R_0$ is the Fresnel Reflection coefficients at normal incidence angle and has a magnitude of about 0.55 at Ku-band for sea surfaces. $S_u^2$ and $S_c^2$ are the variances of surface slopes along and across the wind directions. The last term in the above equation accounts for the decrease of coherent surface reflectivity due to the diffused surface scattering by the small scale roughness with $k_0$ representing the electromagnetic wavenumber and $h$ denoting the standard deviation of small scale roughness. It is evident that $\sigma_{GO}$ decreases as the small scale roughness $h$ increases.

To assess the effects of GO scattering, we have to specify the wind speed dependence of $S_u^2$, $S_c^2$ and $h$. The modulation of small scale waves by long waves is accounted for by assuming an empirical modulation model [9, 10], which has shown a reasonable agreement with several active and passive microwave remote sensing datasets. This model assumes that the small scale roughness is a function of the long wave slope:

$$h^2(S_x) = \sigma^2[1 + f(S_x)] \tag{2}$$

$$f(S_x) = -sgn(S_x)\min(\tfrac{\tan\theta}{S_u}, 0.5) \tag{3}$$

where $\sigma^2$ is the average variance of small scale roughness. $S_x = -\tan\theta$ is the slope of the leeward faces of long waves responding to upwind radar observations and $S_x = \tan\theta$ is the slope of windward faces for downwind radar observations. The function $sgn$ yields 1 $(-1)$ if the argument is positive (negative). This model enhances the roughness of small scale waves on the leeward faces $(S_x < 0)$ and reduces the small scale roughness on the windward faces $(S_x > 0)$.

Taking the ratio of upwind and downwind backscatter from this GO scattering model results in the upwind and downwind asymmetry:

$$\frac{\sigma_{GO}(upwind)}{\sigma_{GO}(downwind)} = \exp[-8k_0^2\sigma^2 f(-\tan\theta)] \tag{4}$$

This ratio is less than unity if $f(-\tan\theta)$ is positive. In other words, the GO scattering provides a negative upwind and downwind asymmetry if the leeward faces have more small scale waves than the windward faces.

It is recognized that the ocean wave spectrum is essentially unknown in the high wind regime. Therefore, we will extrapolate the long wave slope distribution at high winds from Cox and Munk's slope model [8]:

$$S_u^2 = \quad 0.00316U_{125} \tag{5}$$

$$S_c^2 = \quad 0.003 + 0.00192U_{125} \tag{6}$$

where $U_{125}$ is the wind speed at 12.5 m elevation. Regarding the small scale roughness, it has been suggested by [7] that the slope variances of short gravity and capillary waves are proportional to the wind speed at 10 m elevation:

$$s_{GC}^2 = 2.76 \times 10^{-3}U_{10} \tag{7}$$

Because the surface roughness spectrum equals the slope spectrum normalized by the square of wavenumbers, the roughness of short gravity and capillary waves can be approximated by

$$k_0^2\sigma^2 = a \cdot 2.76 \times 10^{-3}U_{10} \tag{8}$$

Since the accuracy of the above roughness model is unknown at hign winds, a tuning constant ($a$) is introduced for a sensitivity analysis.

Fig. 8 illustrates the contributions of GO scattering as a function of wind speed at 35°. 45°, and 55° incidence angles. The upper panel plots the upwind backscattering coefficients for $a = 1$ and 2, indicated by solid and dashed lines. The GO backscatter increases with

increasing wind speeds due to a more likely occurrence of long waves with steep slopes. Comparing the results with a=1 and 2 shows that an increase of small scale roughness reduces the GO surface backscatter. At 45° and 55° incidence angles, the GO backscattering coefficients are significantly lower than the NUSCAT backscatter data (same as those plotted in Fig. 6), suggesting that the GO backscattering has a negligible contribution at moderate and high incidence angles. At 35° incidence angle, the GO scattering becomes more comparable to the NUSCAT data in the high wind regime (above 20 $m \cdot s^{-1}$), and starts to influence the upwind and downwind asymmetry. The lower panel of Fig. 8 illustrates the upwind and downwind asymmetry of GO backscattering coefficients. There could be about -1 to -3 dB asymmetry depending on the small scale roughness. This demonstrates that the GO scattering could lead to a negative upwind and downwind asymmetry at high winds and its influence is larger at smaller incidence angles. However, it should be noted that the effects of GO scattering will be offset by the Bragg scattering by small scale waves, which will bring up the asymmetry. This numerical analysis suggests that the combined contributions from the GO and Bragg scattering may explain the upwind and downwind asymmetry variations with incidence anlges and wind speeds of NUSCAT dual-polarized data.

# 5 Summary

The Ku-band dual-polarized ocean backscatter measurements collected from two sets of aircraft flights are summarized in this paper. The low to moderate wind backscatter data agree well with the NSCAT-1 geophysical model function. A large discrepancy is found between the NSCAT-1 GMF and the aircraft flight data in terms of the wind speed sensitivity of ocean backscatter in the high wind regime. Both polarization channels display modulations of the surface backscatter by wind direction. Horizontal polarization appears to be superior to vertical polarization for wind velocity (speed and direction) measurements for hurricane force winds ($> 32$ $m \cdot s^{-1}$) due to its greater wind speed and direction sensitivity. There is about a change of 2 dB in the horizontally polarized backscatter with the wind speed

increasing from 22 to 35 $m \cdot s^{-1}$. This implies that the hurricane wind speed can be estimated with a 2 $m \cdot s^{-1}$ accuracy, if the radar backscatter measurements can be made accurately to within three tenths of a dB.

A very interesting signature of the ocean backscatter suggested by our aircraft scatterometer study is the upwind and downwind asymmetry of $\sigma_{vv}$ in the high wind regime. An asymmetry of about -0.6 dB was found in the upwind and downwind observations of $\sigma_{vv}$. The conventional view is that the upwind and downwind asymmetry should be positive, as suggested by many aircraft and satellite data acquired at low and moderate wind speeds. A negative asymmetry in the high wind regime appears to contradict the conventional theory that the small scale waves are more concentrated on the leeward faces of long waves. We suggest that this phenomenon is due to the reduction of GO scattering by the small scale waves riding on the long waves. A quantitative analysis was presented with several assumptions about the roughness and slopes of long and short waves. We demonstrate that it is possible to obtain a negative upwind and downwind asymmetry with more concentrated small scale waves on the leeward faces of long waves. However, we offer this model with caution, even though the model signatures appear to agree with the polarization, incidence angle and wind speed dependence of the signals. It should be noted that that our knowledge of the ocean surface spectrum and surface slope distribution remains inadequate at high winds: We do not know how well the Cox and Munk's slope distribution and Hwang's short gravity and capillary wave model [7] would apply at high winds. Other mechanisms such as breaking waves that were not yet well understood could also offer similar backscatter signatures. In-situ or laboratory measurements and more detailed modeling studies are recommended for the characteristics of surface waves and the corresponding electromagnetic scattering problems at high wind speeds.

# 6 Acknowledgment

This work was performed under contract with the National Aeronautics and Space Administration at the Jet Propulsion Laboratory, California Institute of Technology. The comments and assistance by G. Neumann during laboratory tests are critical to a successful laboratory testing of NUSCAT. The authors would like to thank the P-3 aircraft flight crew of the NASA Wallops Flight Facility for assistance in aircraft flight planning and experiments.

[15] W. T. Liu and W. Tang, "Equivalent Neutral Wind," Jet Propulsion Laboratory Publication 96-17, August 1, 1996.

[16] Jessup, A. T., W. C. Keller, and W. K. Melville, "Measurements of Sea Spikes in Microwave Backscatter at Moderate Incidence," *J. Geophys. Res.*, Vol. 95, No. c6, 9679-9688, June 15, 1990.

[17] Bernd Jahne and Klaus S. Riemer, "Two-Dimensional Wave Number Spectra of Small-Scale Surface Waves," *J. Geophy. Res.* Vol. 95, No. C7, 11,531-11,546, July 1990.

[18] Yuguang Liu and Xiao-H. Yan, "The Wind-Induced Wave Growth Rate and the Spectrum of the Gravity-Capillary Waves," *J. of Phy. Oceanography,* Vol. 25, 3196-3218, December 1995.

[19] S. V. Nghiem, F. K. Li, S. H. Lou, G. Neumann, and R. E. McIntosh, "Observations of radar backscatter at Ku and C-Bands in the presence of large waves during the surface wave dynamics experiment," *IEEE Trans. Geosci. and Remote Sensing*, Vol. GE-33, No. 3, 708-721, May 1995.

[20] Carswell, J. R., S. C. Carson, R. E. McIntosh, F. K. Li, G. Neumann, D. Mclaughlin, J. C. Wilkerson, P. G. Black, S. V. Nghiem, "Airborne Scatterometers: Investigating Ocean Backscatter Under Low- and High-Wind Conditions," *IEEE Proceedings,* Vol. 82, No. 12, 1835-1860, December 1994.

[21] A. V. Smirnov and V. U. Zavorotny, "Study of polarization differences in Ku-band ocean radar imagery," *J. of Phy. Oceanography,* Vol. 25, 2215-2228, October 1995.

# List of Tables

| Parameter | Value |
|---|---|
| Frequency (GHz) | 13.95 |
| Antenna Beamwidth (degree) | 3.1 |
| Antenna Gain (dB) | 32 |
| Antenna Sidelobes (dB) | $< -30$ |
| Polarization | VV, HH |
| Transmit Power (W) | 10, 100 |
| Incidence Angle (deg) | 0 to 64 |
| PRF (Hz) | 1500 |
| Frequency Dither Bandwidth (MHz) | 100 |
| Frequency Dither Step (MHz) | 12.5 |
| Radar Sensitivity for 0.5 sec integration time (dB) | 0.2 |
| Aircraft Altitude*** (thousand feet) | 21, 26 |
| Absolute calibration (dB) | <1 |
| Calibration Stability (dB) | <0.2 |
| Scan Mode | Fixed pointing, Azimuth scan |
| Nominal Aircraft Ground Track Speed (Knot) | 200 |

Table 1: NUSCAT key parameters for the aircraft HOWE campaign conducted in September 1997.

# List of Figures

# GPS DROPSONDE MEASUREMENTS FROM NUSCAT FLIGHTS OVER HURRICANE ERIKA

## 970911 170255/193357

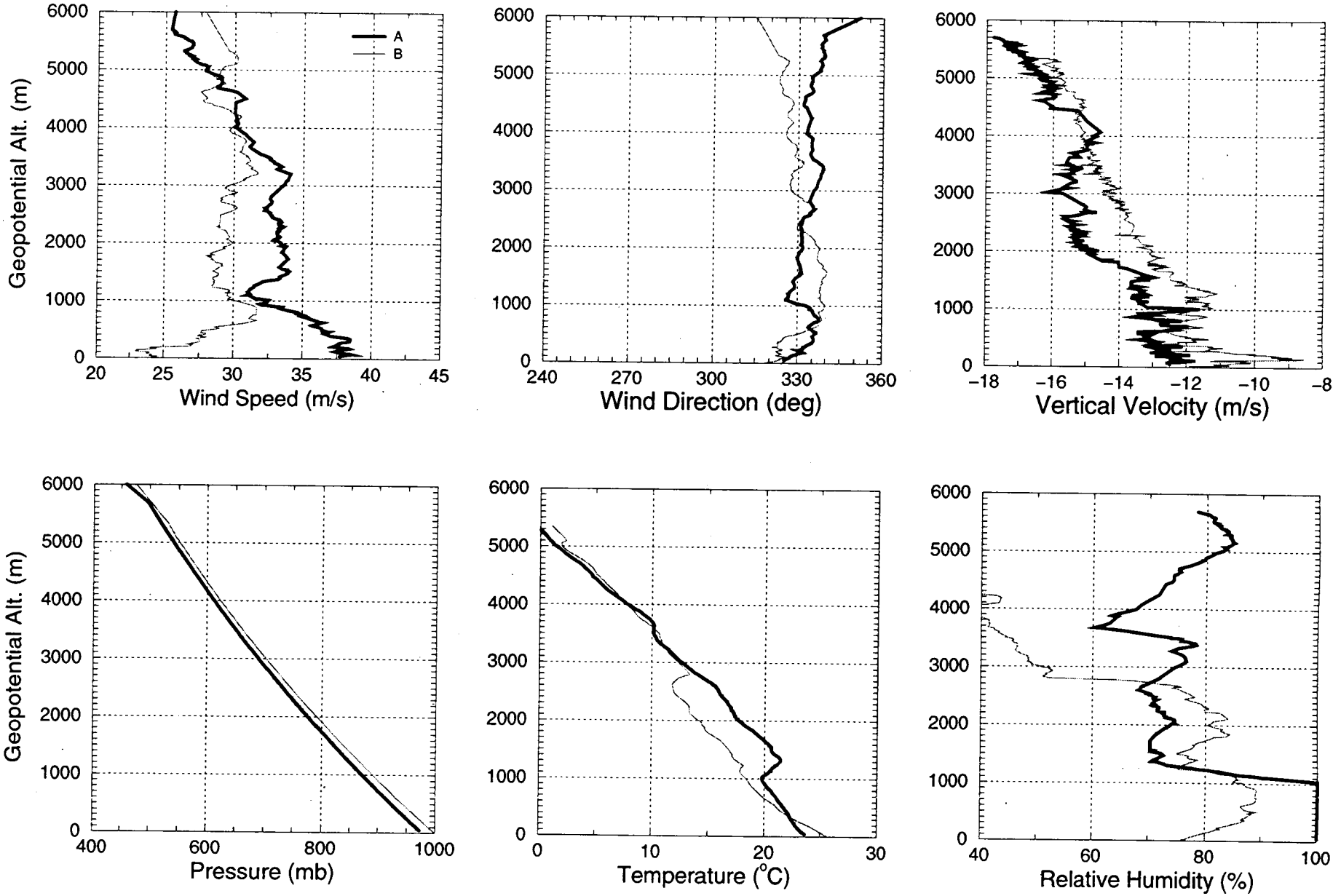


Fig. 1

# NSCAT-1 MODEL FUNCTION AND NUSCAT DATA

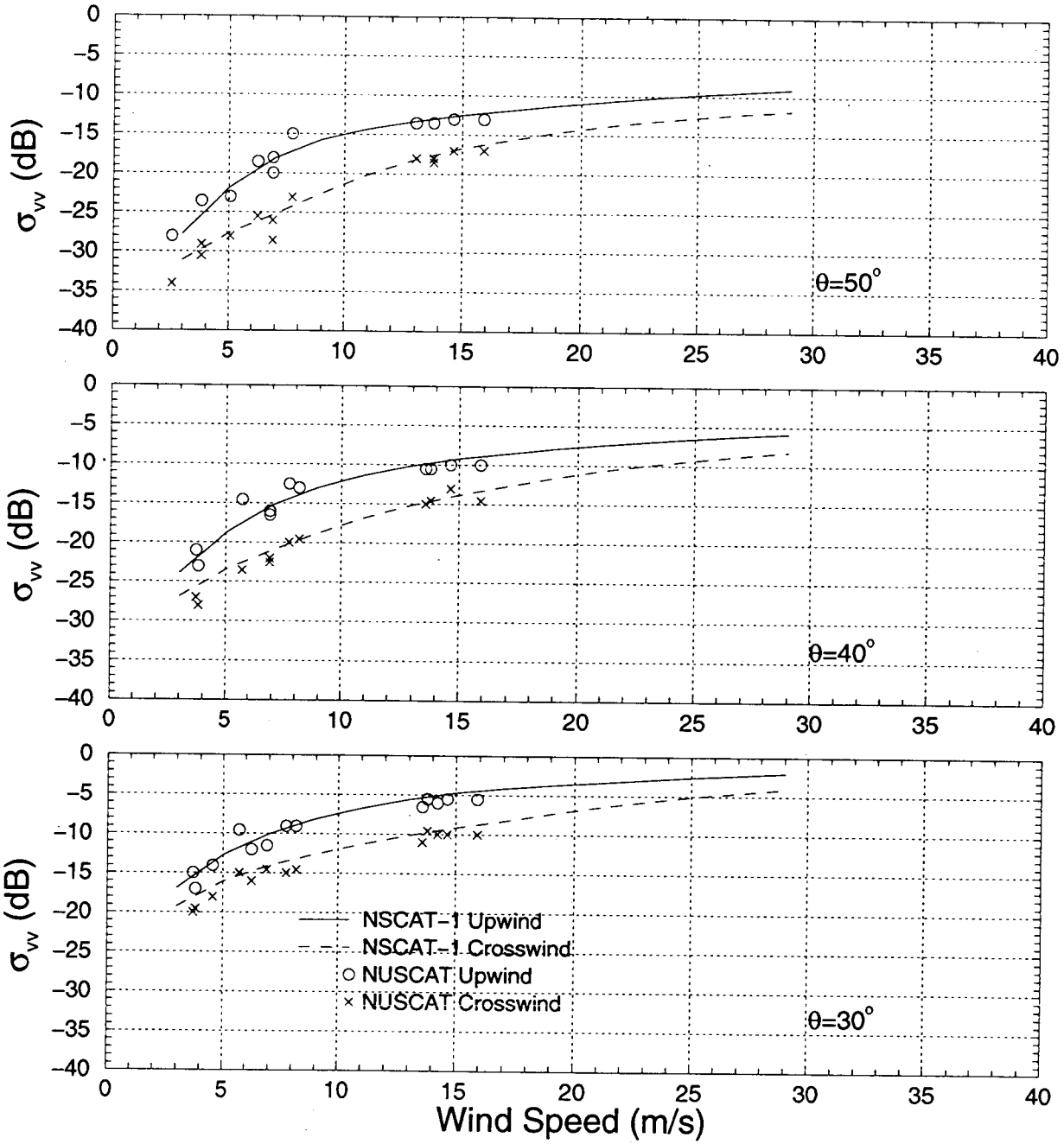


Fig 2

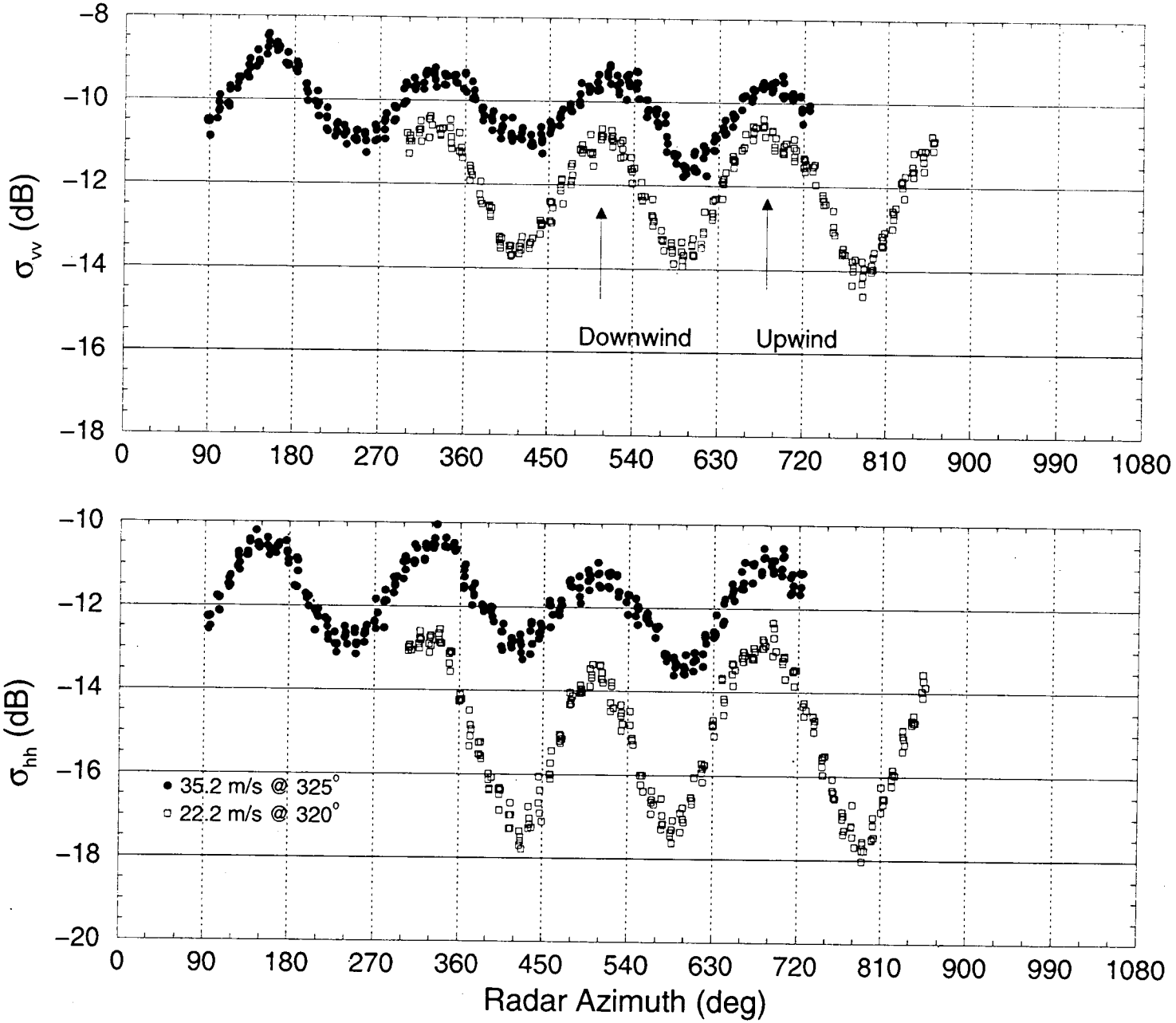
−8
−10
−12
−14
−16
−18
$\sigma_{vv}$ (dB)
Downwind
Upwind
0
90
180
270
360
450
540
630
720
810
900
990
1080
−10
−12
−14
−16
−18
−20
$\sigma_{hh}$ (dB)
• 35.2 m/s @ 325°
□ 22.2 m/s @ 320°
Radar Azimuth (deg)

Fig. 3

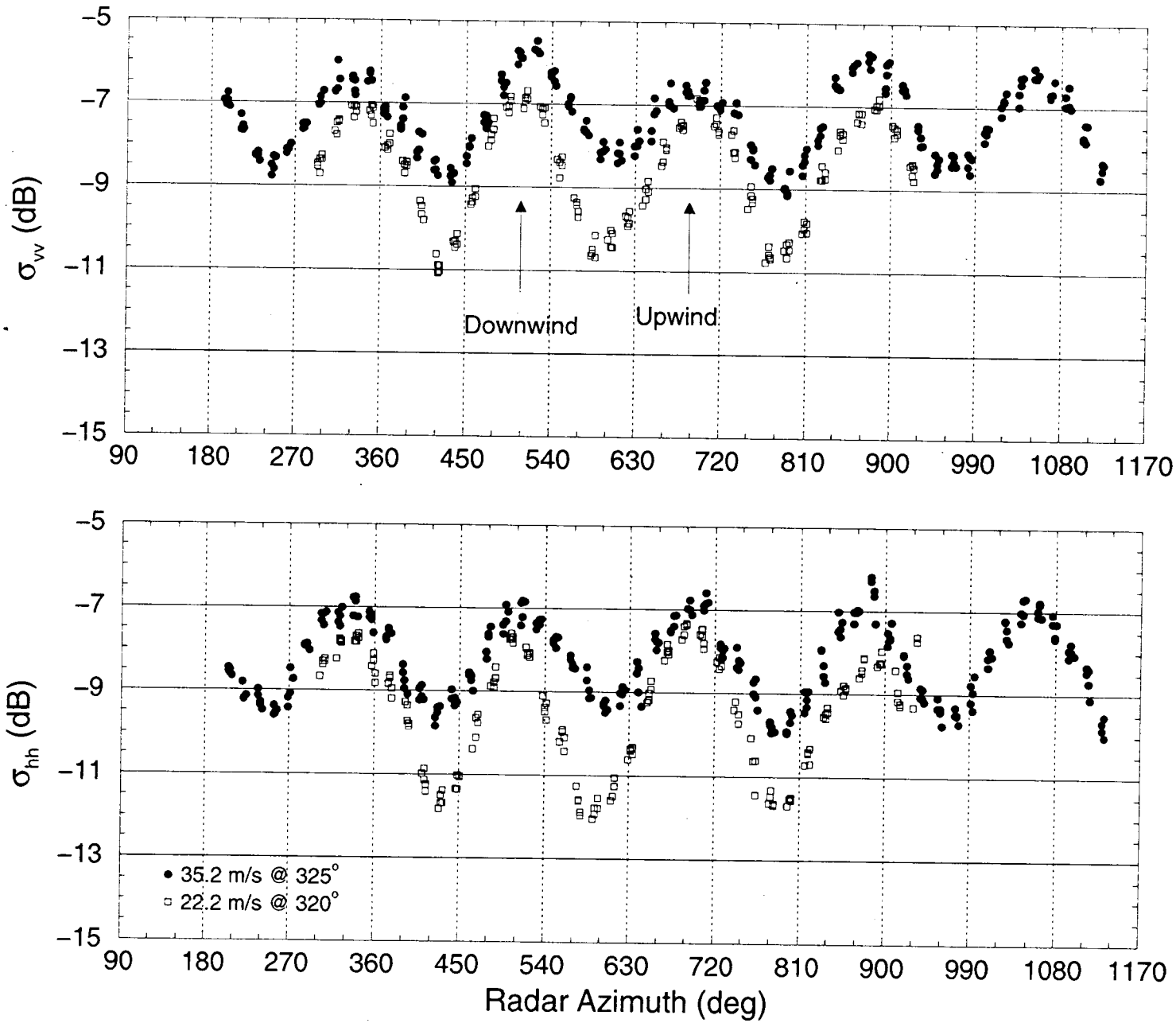
−5
−7
−9
−11
−13
−15
σvv (dB)
Downwind
Upwind
90
180
270
360
450
540
630
720
810
900
990
1080
1170
σhh (dB)
• 35.2 m/s @ 325°
▫ 22.2 m/s @ 320°
Radar Azimuth (deg)

Fig. 2

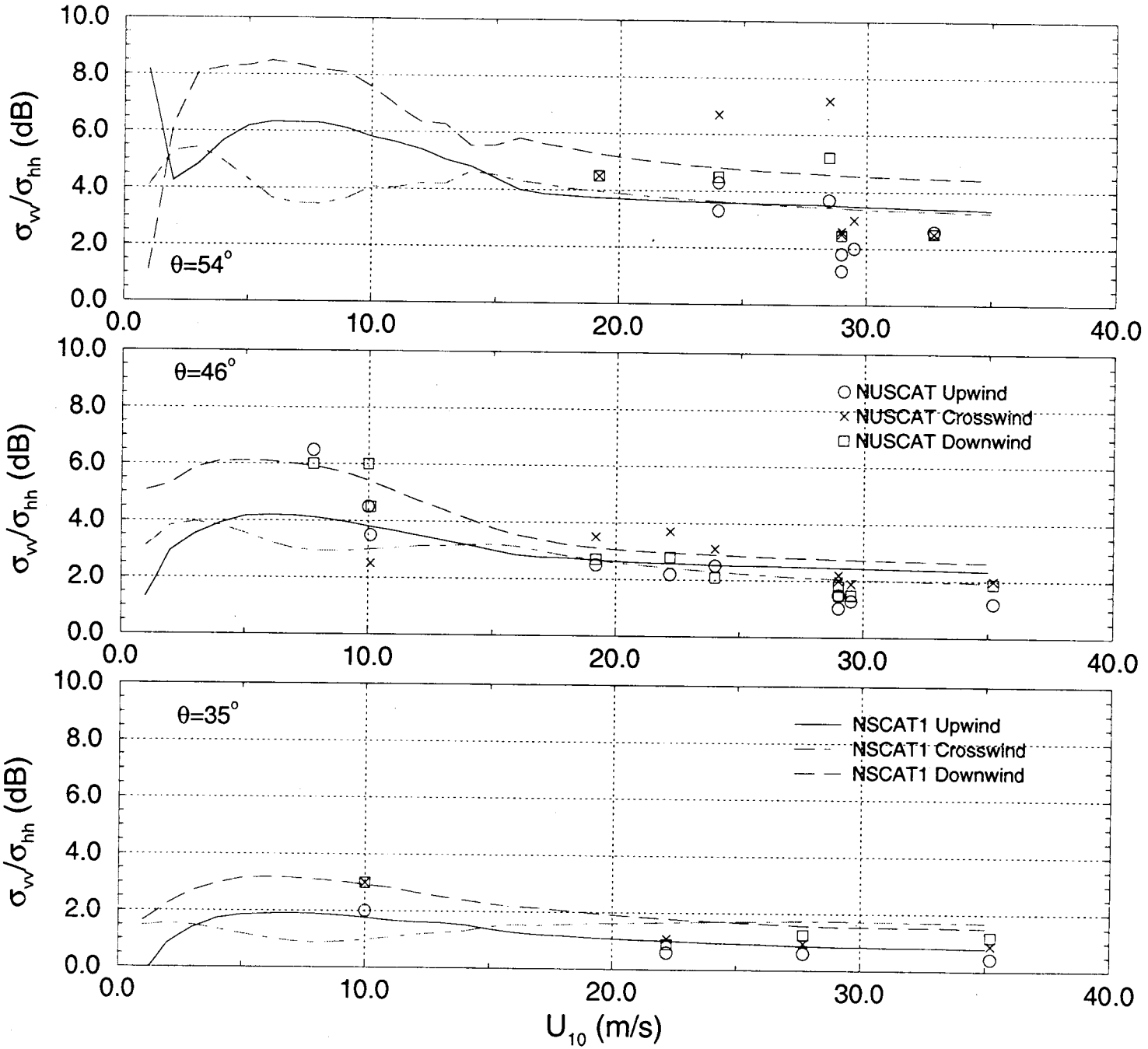
10.0
8.0
6.0
4.0
2.0
0.0
$\sigma_{vv}/\sigma_{hh}$ (dB)
θ=54°
θ=46°
θ=35°
NUSCAT Upwind
NUSCAT Crosswind
NUSCAT Downwind
NSCAT1 Upwind
NSCAT1 Crosswind
NSCAT1 Downwind
0.0
10.0
20.0
30.0
40.0
$U_{10}$ (m/s)

Fig 5

# COMPARISON OF NSCAT-1 MODEL FUNCTION AND NUSCAT OBSERVATIONS OF HURRICANE ERIKA

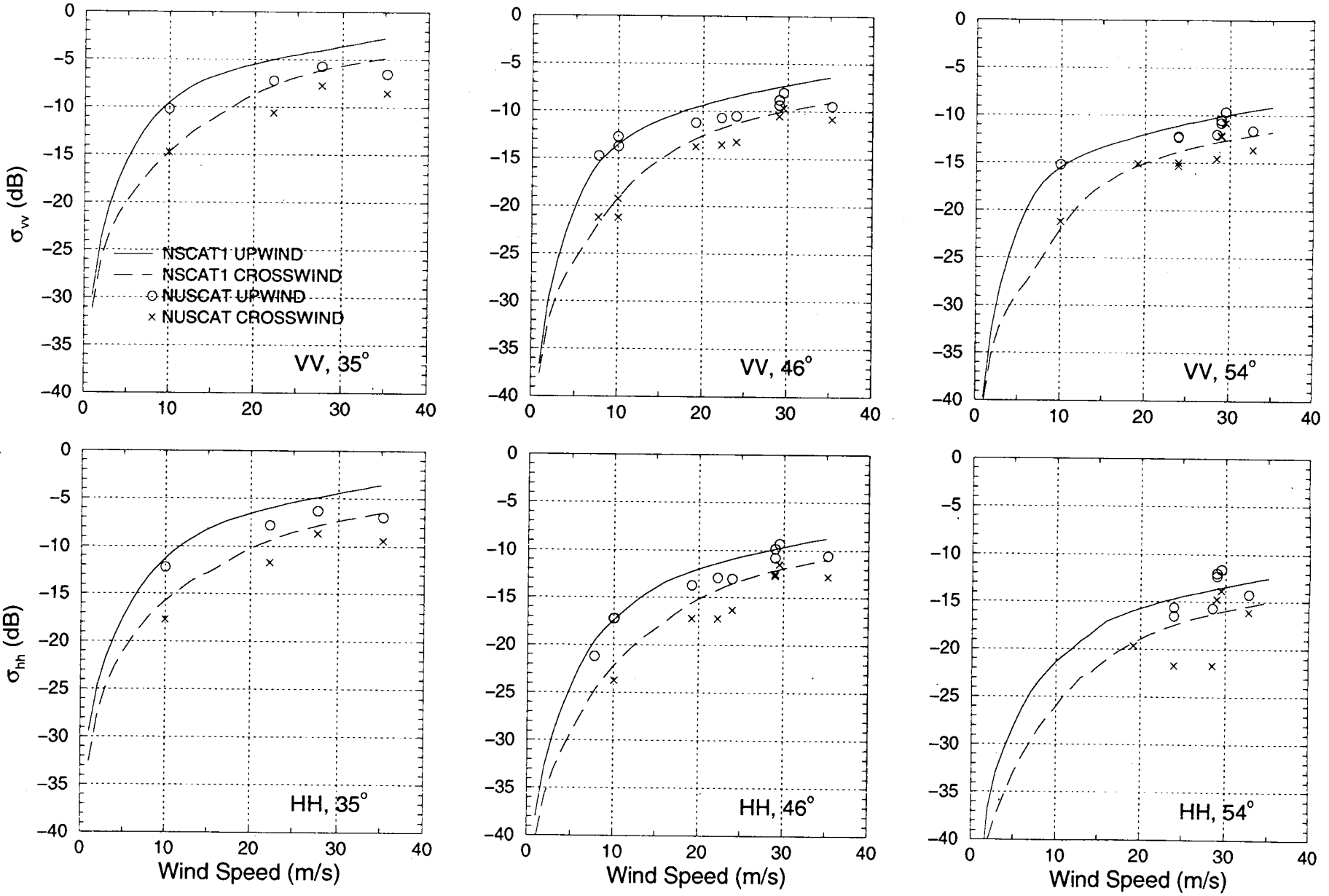


Fig 6

# NSCAT–1 MODEL FUNCTION AND NUSCAT OBSERVATIONS

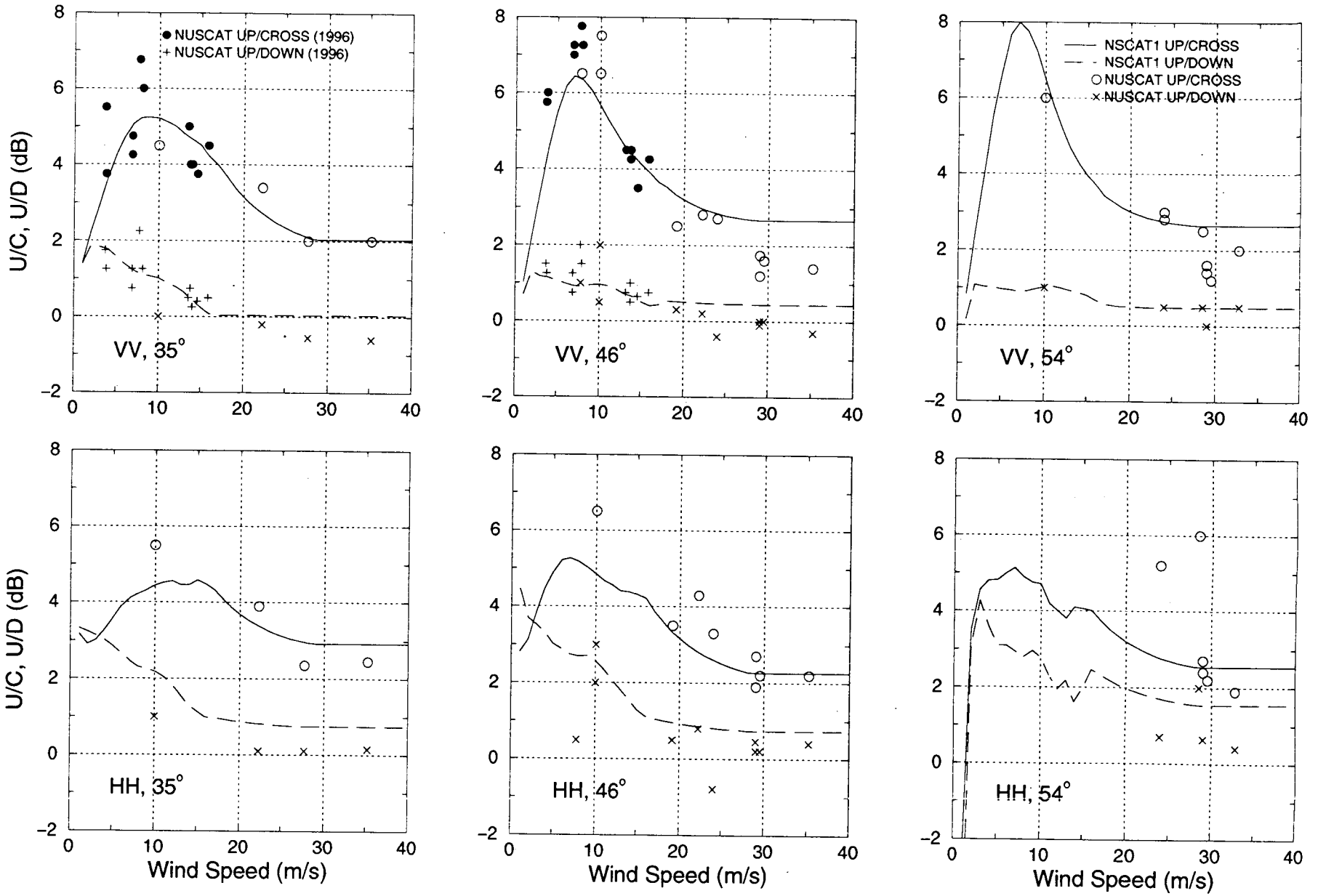

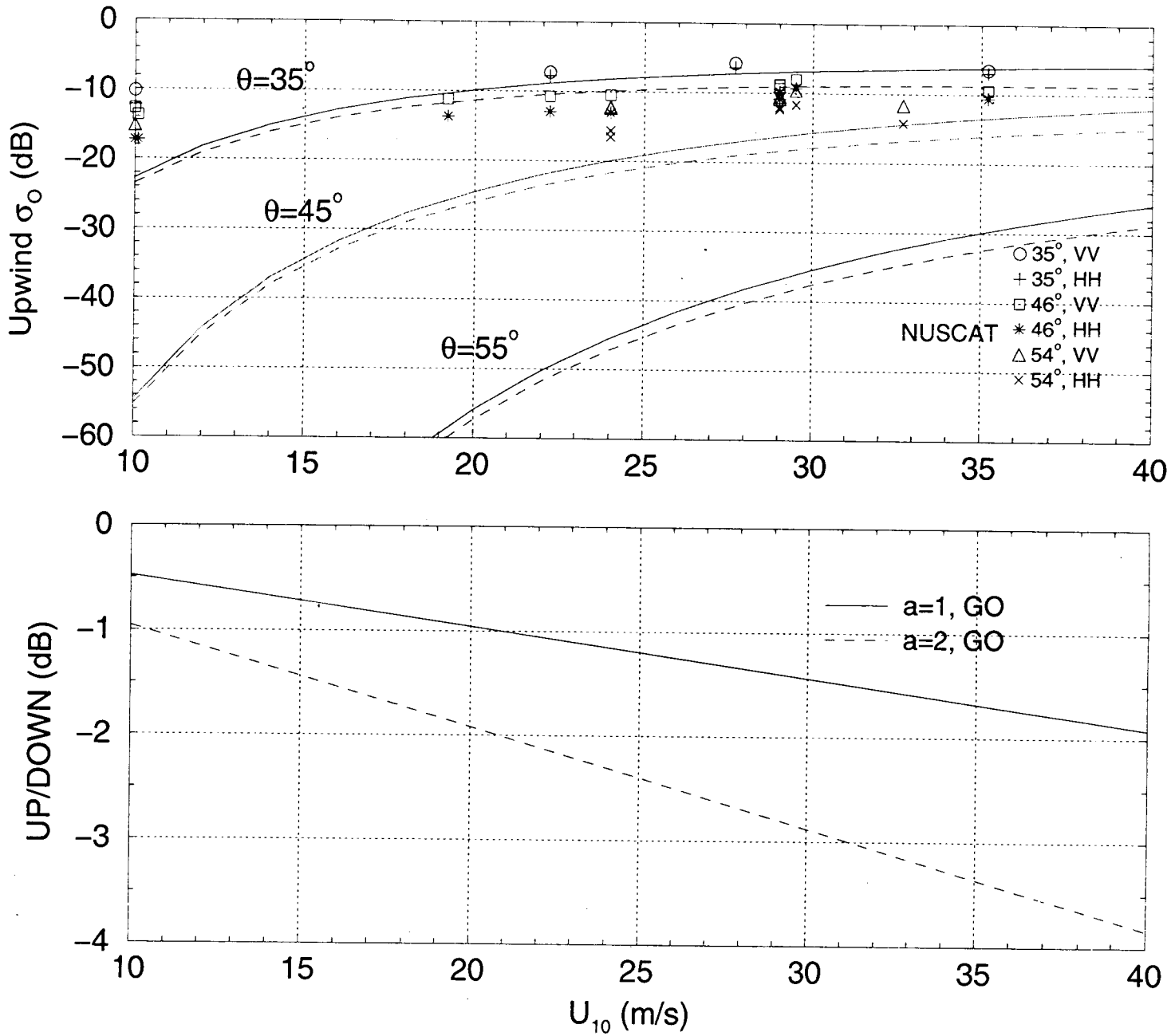
Upwind $\sigma_o$ (dB)
0
−10
−20
−30
−40
−50
−60
θ=35°
θ=45°
θ=55°
NUSCAT
35°, VV
35°, HH
46°, VV
46°, HH
54°, VV
54°, HH
10
15
20
25
30
35
40
UP/DOWN (dB)
0
−1
−2
−3
−4
a=1, GO
a=2, GO
$U_{10}$ (m/s)

Fig. 8